




Composite spiral waves in discrete-time systemsXin Wang ^{1,2,3} Jian Gao ^{1,2,3,*} Changgui Gu,⁴ Daiyong Wu,^{1,2,3} Xinshuang Liu,^{1,2,3} and Chuansheng Shen ^{1,2,3}¹*International Joint Research Center of Simulation and Control for Population Ecology of Yangtze River in Anhui, Anqing Normal University, Anqing 246011, People's Republic of China*²*Key Laboratory of Modeling, Simulation and Control of Complex Ecosystem in Dabie Mountains of Anhui Higher Education Institutes, Anqing Normal University, Anqing 246011, People's Republic of China*³*School of Mathematics and Physics, Anqing Normal University, Anqing 246011, People's Republic of China*⁴*Business School, University of Shanghai for Science and Technology, Shanghai 200093, People's Republic of China*

(Received 2 February 2023; revised 29 April 2023; accepted 18 September 2023; published 6 October 2023)

Spiral waves are a type of typical pattern in open reaction-diffusion systems far from thermodynamic equilibrium. The study of spiral waves has attracted great interest because of its nonlinear characteristics and extensive applications. However, the study of spiral waves has been confined to continuous-time systems, while spiral waves in discrete-time systems have been rarely reported. In recent years, discrete-time models have been widely studied in ecology because of their appropriateness to systems with nonoverlapping generations and other factors. Therefore, spiral waves in discrete-time systems need to be studied. Here, we investigated a novel type of spiral wave called a composite spiral wave in a discrete-time predator-pest model, and we revealed the formation mechanism. To explain the observed phenomena, we defined and quantified a move state effect of multiperiod states caused by the coupling of adjacent stable multiperiod orbits, which is strictly consistent with the numerical results. The other move state effect is caused by an unstable focus, which is the state of the local points at the spiral center. The combined effect of these two influences can lead to rich dynamical behaviors of spiral waves, and the specific structure of the composite spiral waves is the result of the competition of the two effects in opposite directions. Our findings shed light on the dynamics of spiral waves in discrete-time systems, and they may guide the prediction and control of pests in deciduous forests.

DOI: [10.1103/PhysRevE.108.044205](https://doi.org/10.1103/PhysRevE.108.044205)**I. INTRODUCTION**

Spiral wave patterns are a type of typical spatiotemporal structure in open systems far from thermodynamic equilibrium. Spiral wave patterns are spirals that steadily rotate in time, which can self-organize and self-sustain with the spiral tip as the wave source [1]. They are often observed in oscillatory and excitable media, such as chemical reactions [2–6], populations of micro-organisms [7,8], planar semiconductor-gas discharge systems [9], catalytic reactions on the surface of Pt(110) [10,11], liquid crystal systems [12], cardiac tissue systems [13,14], and fluid convection [15]. The study of spiral waves has attracted a great deal of attention due to their nonlinear characteristics and potential applications [16,17]. For instance, the study of spiral waves in the spatial distribution of pests can guide pest control services [2,18]. What is more, spiral waves and fragments of electric signals in cardiac tissue are the main cause of tachycardia and ventricular fibrillation, respectively [19,20]. In addition, spiral waves in the cerebral cortex may be related to the irregular seizures that occur with epilepsy [21].

The discovery of spiral waves with novel structures, and the understanding of their formation mechanisms, are focuses of research on pattern formation [16]. Many types of spiral

waves have been found and studied in experiments, numerical simulations, and theoretical studies in the past three decades, including superspiral waves [16,22,23], ripple waves [24,25], segmented waves [26,27], overtargeted waves [28,29], anti-spiral waves [30], wavelength-doubled waves [31], period-doubled waves [32,33], and super multiarmed and segmented (SMAS) spiral waves [34]. However, the studies of spiral waves have generally been limited to continuous-time systems, which are described by differential equations, while spiral waves in discrete-time systems have been rarely reported. Discrete-time and spatial implicit population models, which can be described by difference equations, have been widely investigated in recent years, mainly because when the population number is small or populations have nonoverlapping generations, the discrete-time models are more realistic than the continuous-time ones, and more accurate numerical results can be obtained from discrete-time models [35–42]. In particular, discrete-time and spatial implicit predator-prey models consisting of two species have been extensively investigated [43–47]. Spatial explicit models are more realistic than spatial implicit models for ecosystem prediction [48], and discrete-time spatial explicit predator-prey models are rarely reported. Therefore, it is of great ecological values to investigate spatiotemporal patterns, especially spiral waves, in discrete-time spatial explicit predator-prey models.

In this article, we investigated a new type of spiral wave, called the composite spiral wave, in a spatial explicit

*Corresponding author: gaojian1612@163.com

discrete-time model. The combined effect of the two move state effects can lead to rich dynamical behaviors of spiral waves, and the composite spiral waves are the results of the competition between the two effects in opposite directions. The rest of the article is organized as follows. Section II introduces the model and method, Sec. III shows the numerical results, and Sec. IV presents the analytical results. Conclusions and discussions are presented in Sec. V.

II. MODEL AND METHOD

Discrete-time population models, described by difference equations, have been widely investigated in recent years. They are more realistic than continuous-time ones when the populations have nonoverlapping generations or the number populations is small [40]. Nonoverlapping generations are the reproductive characteristics of organisms that live for only one year and reproduce only once a year, such as annual plants and many insects.

We considered the dynamics of a predator-pest model in warm-temperate deciduous forests, where the predators and pests are both insects with nonoverlapping generations. The model is constructed as follows. When only considering birth rate and environmental capacity, the population density of insects with nonoverlapping generations can be described by the logistic map

$$p_{n+1} = \mu_p p_n (1 - p_n), \quad \mu_p > 0. \quad (1)$$

p_n is the population density of insects in the n th generation. The fluctuations in the population densities of predators and pests near an equilibrium point are denoted as α and β , respectively. Because the food resources of predators near the equilibrium point are generally insufficient, the interaction between/among predators is mainly manifested as competition, resulting in a suppression of the n th to the $(n+1)$ th generation of predators. Pests, the food of predators, exhibit a contribution to predators of the same generation as pests. Suppression and contribution are considered to be linear and subject to linear superposition, i.e.,

$$\alpha_{n+1} = -a\alpha_n + a'\beta_{n+1}, \quad (2)$$

where a ($a > 0$) is the self-suppression coefficient of predators, and a' ($a' > 0$) is the other-contribution coefficient of pests.

The food resources of pests are generally sufficient, and the interaction between pests is manifested as reproduction, so the n th generation of pests contributes positively to the next generation. Food resources of pests are generally sufficient, so the interaction between/among pests is mainly manifested as reproduction, resulting in a contribution of the n th to the $(n+1)$ th generation of pests. Considering the suppression of predators to pests in the same generation, the following relationship can be obtained:

$$\beta_{n+1} = -d'\alpha_{n+1} + d\beta_n. \quad (3)$$

Here, d ($d > 0$) is the self-contribution coefficient of pests, and d' ($d' > 0$) is the other-suppression coefficient of predators. The parameter d is mainly derived from the birth rate of pests.

Using Eq. (1) to estimate α_{n+1} in Eq. (3) and β_{n+1} in Eq. (2), one can obtain

$$\begin{aligned} \alpha_{n+1} &= f(\alpha_n, \beta_n) = -a\alpha_n + b\beta_n(1 - \beta_n), \\ \beta_{n+1} &= g(\alpha_n, \beta_n) = -c\alpha_n(1 - \alpha_n) + d\beta_n. \end{aligned} \quad (4)$$

The parameters b and c represent $a'\mu_\beta$ and $d'\mu_\alpha$, respectively. When the area of a deciduous forest is large enough, the vertical differences can be ignored, and the deciduous forest can be regarded as a two-dimensional (2D) plane system. Considering spatial heterogeneity and the fact that the mobility of winged predators is much greater than that of wingless pests, Eq. (4) can be rewritten as a spatially extended discrete-time model [49], which reads

$$\begin{aligned} \alpha_{n+1} &= f(\alpha_n, \beta_n) + D\nabla^2\alpha_n, \\ \beta_{n+1} &= g(\alpha_n, \beta_n), \end{aligned} \quad (5)$$

where ∇^2 is $\partial^2/\partial x^2 + \partial^2/\partial y^2$. D represents the diffusion coefficient of predators, and the diffusion coefficient of pests is approximately equal to 0. The parameter d ($1.500 \leq d \leq 1.554$) was chosen as the control parameter. The other parameters were fixed: $a = 1$, $b = 9/10$, and $c = 16/5$. The vectorial map of Eq. (5) is

$$\begin{aligned} \mathbf{X}_{n+1} &= \begin{bmatrix} \alpha_{n+1} \\ \beta_{n+1} \end{bmatrix} = \mathbf{G} \begin{bmatrix} \alpha_n \\ \beta_n \end{bmatrix} = \mathbf{G}(\mathbf{X}_n) \\ &= \begin{bmatrix} f(\alpha_n, \beta_n) + D\nabla^2\alpha_n \\ g(\alpha_n, \beta_n) \end{bmatrix}. \end{aligned} \quad (6)$$

Simulations of this model were carried out on 300×300 grid points with *no-flux* boundary conditions. The boundary conditions can be expressed as $\mathbf{n} \cdot \nabla\alpha = \mathbf{0}$, where \mathbf{n} is a vector normal to the system boundary. The approximate method is the same as in Ref. [50] (see the MATLAB codes in the supplemental material). The method to discretize the Laplacian terms $\nabla^2\alpha$ was a nine-point finite-difference scheme. Specifically, the variables on the grid points are calculated as follows:

$$\alpha_{n+1}^{i,j} = f(\alpha_n^{i,j}, \beta_n^{i,j}) + \frac{D}{h^2} \sum_{i'=i-1}^{i+1} \sum_{j'=j-1}^{j+1} M^{i',j'} \alpha_n^{i,j}, \quad (7)$$

$$\beta_{n+1}^{i,j} = g(\alpha_n^{i,j}, \beta_n^{i,j}),$$

$$(i, j = 1, 2, 3, \dots, 300),$$

with

$$\mathbf{M} = \frac{1}{6} \begin{bmatrix} 1 & 4 & 1 \\ 4 & -20 & 4 \\ 1 & 4 & 1 \end{bmatrix}.$$

The scaled diffusion coefficient D/h^2 was 0.1 (h is the spatial step).

III. NUMERICAL RESULTS

Within the parameter interval considered in this article ($1.500 \leq d \leq 1.554$), the spatially homogeneous system of Eq. (5) exhibits period-5 oscillations (see Fig. S1 of the Supplemental Material [51]). To simplify the problem, we can

directly describe the period-5 states, which can be determined by the vectorial map

$$\begin{aligned} \mathbf{r}_{n+1} &= \begin{bmatrix} \alpha_{n+1} \\ \beta_{n+1} \end{bmatrix} = \mathbf{G} \circ \mathbf{G} \circ \mathbf{G} \circ \mathbf{G} \circ \mathbf{G}(\mathbf{r}_n) \\ &= \mathbf{G}^5(\mathbf{r}_n) = \mathbf{G}^5 \begin{bmatrix} \alpha_n \\ \beta_n \end{bmatrix}, \end{aligned} \quad (8)$$

where “ \circ ” represents a compound operation, and the exponent in the upper right corner of \mathbf{G} does not represent power but represents the number of compound operations. For instance, $\mathbf{G} \circ \mathbf{G}(\mathbf{X}_n) = \mathbf{G}^2(\mathbf{X}_n) = \mathbf{G}[\mathbf{G}(\mathbf{X}_n)]$.

Our previous study has found that by adjusting the value of the parameter d , the structure of the spiral wave can be suddenly changed. To explore the mechanism that leads to the abrupt change of structure of the spiral wave, we need to observe the evolution process of structure with the change of the parameter d . As shown in Fig. 1, when the parameter d is equal to 1.5000, the system supports a common (outward-propagating) spiral wave [see Video 1 [51]]. When d is equal to 1.5440, the structure of the pattern does not change, but the waves no longer propagate, and the pattern is a static spiral structure [see Fig. 1(b) and Video 2 [51]]. It can be seen that this spiral pattern is generated by the movement of boundaries between neighboring cells. As the range of the inner spiral increases, the moving boundaries disappear at the edge of the 2D system, so that the inner spiral pattern cannot fill the entire system. When d is equal to 1.5450, one can obtain an inward-propagating spiral wave [see Fig. 1(c) and Video 3 [51]]. When d is equal to 1.5455, the final structure of the pattern changes [see Fig. 1(d4) [51]]. In the final structure, a small spiral (SS) occupies the central area of the pattern, and a bigger spiral (BS) outside the SS is composed of five spiral cells, with sharp boundaries existing between neighboring cells. The values of the five cells correspond to the five stable period-5 orbits, respectively. In addition, the SS is an inward-propagating spiral wave, while the BS is an outward-propagating spiral wave (see Video 4 [51]). Because this type of spiral wave is a combination of the SS and BS, we named it the composite spiral wave (CSW). When the parameter d is increased to 1.5500, in the final structure, the wavelength of the BS and the size of the SS both become smaller [see Fig. 1(e4) and Video 5 [51]]. Specifically, the wavelength of the CSW is specified as the wavelength of the BS. The calculation method for the wavelength λ of spiral waves is shown in Fig. 1(e4). The wavelength λ of the CSWs contains five “cell-widths” λ_b , i.e., $\lambda = 5\lambda_b$. The “cell-width” refers to the width of the spiral cells [see Fig. 1(d4) for an example]. Therefore, when the wavelength λ of the CSWs is too large to be directly measured, we can indirectly obtain λ by measuring λ_b . The wavelength of the CSWs is proportional to the diameter of the area occupied by the SS, i.e.,

$$\lambda = \pi \Phi_{SS}, \quad (9)$$

where Φ_{SS} represents the diameter of the area occupied by the SS. For instance, the area occupied by the SS in Fig. 1(d4) is marked by a red circle. The circle is centered around the spiral tip of the SS and passes through the points of maximum curvature at the boundaries between neighboring cells.

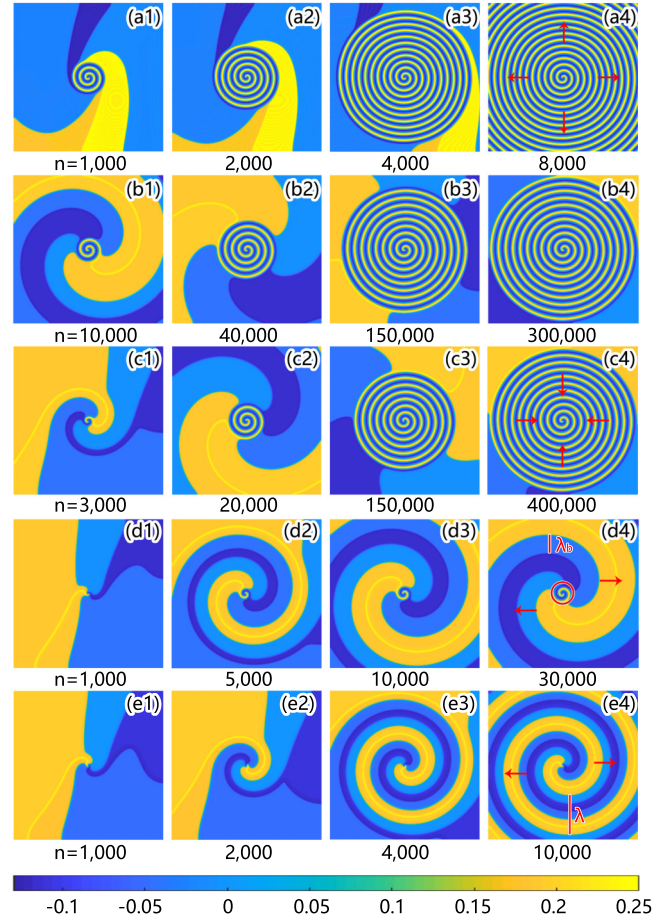


FIG. 1. Spiral waves (the spatial distribution of the variable β , i.e., invasive alien pests, in the 2D system) with different values of the parameter d : (a) $d = 1.5000$, (b) $d = 1.5440$, (c) $d = 1.5450$, (d) $d = 1.5455$, and (e) $d = 1.5500$. The initial values are $\alpha_0^{i,j} = 0.01(j/300 - 0.005)$ and $\beta_0^{i,j} = 0.01(i/300 - 0.005)$. Each spiral wave has reached the final structure. The red circle in (d4) indicates the area occupied by the SS. The λ_b in (d4) represents the width of the spiral cell, and the λ in (e4) is the wavelength of the spiral wave. The patterns in (a4), (b4), (c4), (d4), and (e4) all reached their final structures. The red arrows indicate the propagation direction waves.

The mechanism of Eq. (9) is as follows. The boundaries move at the same speed. When the spiral wave experiences a period, each boundary near the circle moves around the circle once, and at the same time, the wave propagates a distance of one wavelength forward. Therefore, the wavelength is equal to the circumference of the circle. The wavelengths of the outward-propagating spiral wave, static spiral, inward-propagating spiral wave, and SS are the same. Note that the wavelength λ in this article refers to the wavelength of a spiral that reaches the final structure.

In fact, the inward-propagating spiral in Fig. 1(c4) is also the CSW. The corresponding BS cannot be displayed because the SS almost occupies the entire 2D rectangular system. Like the static spiral in Fig. 1(b), the inward-propagating spiral wave is also formed by the boundary winding around the spiral center. The winding of the boundary causes the spiral to expand, while the inward propagation causes it to shrink.

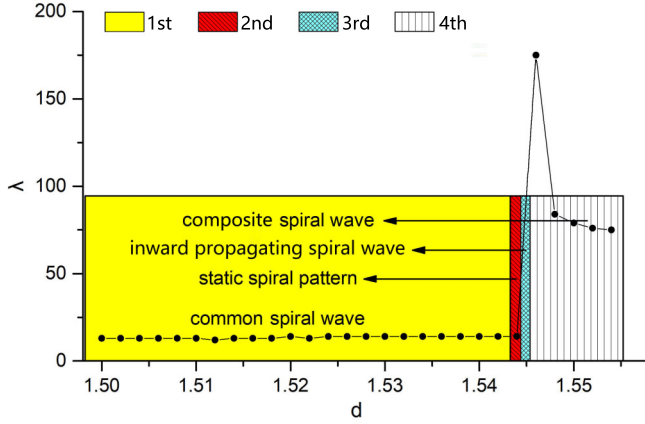


FIG. 2. Detailed changes of wavelength and structure for spiral waves in the parameter interval $d \in [1.500, 1.554]$. Inset: partial enlarged drawing. The interval of d $[1.500, 1.554]$ is divided into four parts, i.e., the first interval $[1.5000, 1.5438]$, the second interval $[1.5438, 1.5446]$, the third interval $(1.5446, 1.5454]$, and the fourth interval $(1.5454, 1.5540]$.

One can obtain the relationship

$$\nu_b T_s = \pi \Phi_{SS},$$

where ν_b is the speed of the boundary, T_s is the period of the inward-propagating spiral wave, and Φ_{SS} is the diameter of the area occupied by the inward-propagating spiral wave. This equation describes the relationship when the circular area occupied by the inward-propagating spiral wave reaches stability. When the wave propagates inward for a wavelength (passing through a period), the boundary also needs to circle the circular area once. The diameter of the circular area can be obtained as

$$\Phi_{SS} = \frac{\nu_b T_s}{\pi}. \quad (10)$$

It can be seen that the inward-propagating spiral has a specific size. Therefore, the inward-propagating spiral we observed is only the central region of the CSW.

We need to obtain more detailed information on the effects of the parameter d on spiral waves. Figure 2 describes the detailed changes in the wavelength and structure of spiral waves in the parameter interval $d \in [1.500, 1.554]$. When the CSWs do not appear ($d \in [1.5000, 1.5454]$, i.e., the first, second, and third intervals), the wavelengths corresponding to different values of the parameter d are the same. Specifically, in the first interval ($d \in [1.5000, 1.5438]$), the patterns are common outward-propagating spiral waves. In the second interval ($d \in [1.5438, 1.5446]$), the patterns are static spirals. In the third interval ($d \in (1.5446, 1.5454]$), the patterns are inward-propagating spiral waves. When the parameter d increases to the fourth interval initially, the CSW with SS and BS appears. As d continues to increase, the area occupied by the SS decreases. At the same time, the wavelength of the CSW also decreases.

Understanding the formation process of the spiral wave may help us understand the formation mechanism. Figure 3 shows the formation processes of spiral waves [initial conditions can be found in Fig. 3(a1)]. When the parameter

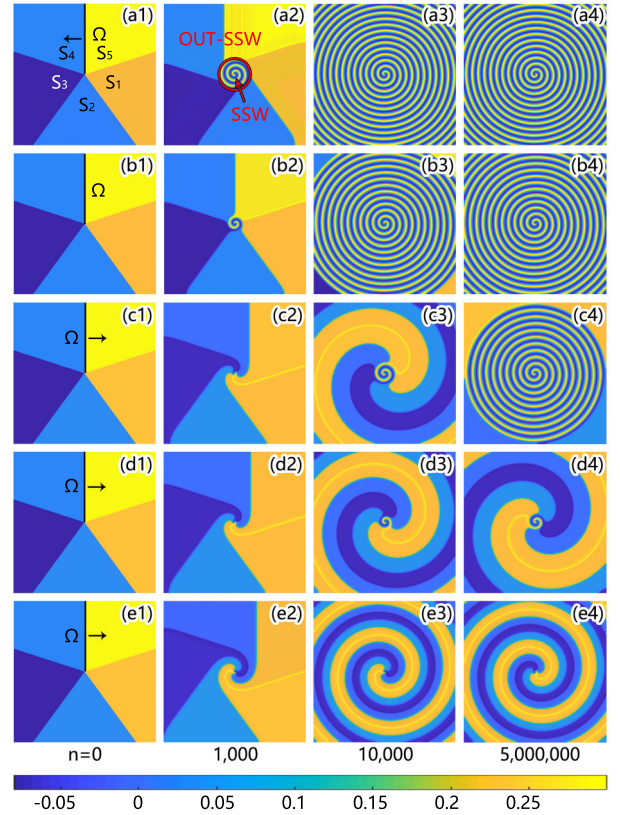


FIG. 3. Processes of formation for spiral waves with different values of d : (a) $d = 1.5000$, (b) $d = 1.5212$, (c) $d = 1.5440$, (d) $d = 1.5455$, and (e) $d = 1.5500$. In (a1), (b1), (c1), (d1), and (e1), the lines Ω are marked boundaries (the boundary between different states), and the others are not marked. The black arrows indicate the moving direction of Ω . In particular, the boundaries in (b) are stationary. Initial conditions are shown in (a1): $S_1 = (\alpha, \beta) = (0.1048, 0.1835)$, $S_2 = (0.0301, -0.0250)$, $S_3 = (-0.0531, -0.1307)$, $S_4 = (-0.0799, -0.0172)$, $S_5 = (0.0642, 0.2504)$.

d is equal to 1.5000, the boundary Ω moves to the left and gradually forms an outward-propagating spiral wave [see (a) and Video 6 [51]]. When d is in the interval $[1.5202, 1.5234]$, the boundary Ω does not move, and an outward-propagating spiral wave appears in the center [see (b) and Video 7 [51] for an example]. When d is equal to 1.5440, the boundary Ω moves to the right and forms a static spiral pattern in the center [see (c) and Video 8 [51]]. When d equals 1.5455, the boundary Ω moves to the right and a CSW can be formed [see (d) and Video 9 [51]]. When d is equal to 1.5500, the boundary Ω moves to the right and a CSW with a smaller SS is formed [see (e) and Video 10 [51]]. In fact, the movement of the boundaries is an external manifestation of the movement of the period-5 states in the phase space. Therefore, we need to have a specific understanding of the dynamical behaviors of local points.

We examined the dynamical behaviors of local points in different regions during the formation of spiral waves. During the formation, the pattern can be divided into two parts: the spiral with small wavelength (SSW) at the center, and the other part outside the SSW (OUT-SSW). For instance, the

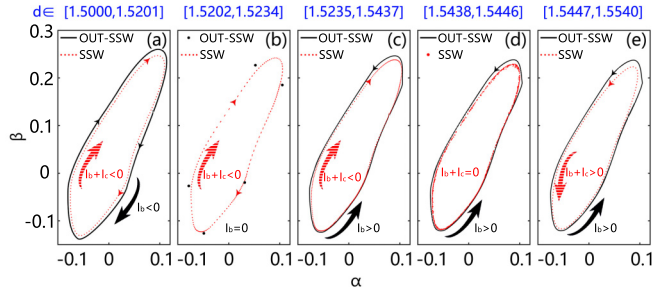


FIG. 4. The dynamical behaviors of local points vary with the value of d : (a) $d = 1.5000$, (b) $d = 1.5212$, (c) $d = 1.5300$, (d) $d = 1.5440$, and (e) $d = 1.5455$. In (a), (c), (d), and (e), the black curves are invariant circles of the period-5 states of local points in the OUT-SSW. In (b), the period-5 states of local points in the OUT-SSW are stable in period-5 orbits. In (a)–(c), and (e), the red dotted curves are invariant circles of the period-5 states of local points in the SSW. In (d), the period-5 states of local points in the SSW form a closed curve in the phase space. The arrows on invariant circles represent the movement direction of the period-5 states. The bigger black arrows represent the direction of I_b . The bigger red arrows represent the direction of the combined effect of I_b and I_c . The interval above each figure represents the interval of d with the same dynamical behavior.

spiral inside the red circle in Fig. 3(a2) is the SSW, and the other part is the OUT-SSW. Note that the SSW refers to the inner spiral with a smaller wavelength during the formation, and the SS refers to the small spiral in the final structure of the CSWs. Specially, in the CSWs, the SS is an SSW that reaches the final structure. The dynamical behaviors of local points are shown as follows.

Figure 4 describes the dynamical behaviors of local points with different values of d ($d \in [1.500, 1.554]$). The results show that the dynamical behaviors of local points in the SSW are different from those in the OUT-SSW. In spiral waves other than the CSWs, the boundaries gradually disappear in the formation processes of spiral waves. In the final structures of these spiral waves, except for the local points at the center of the spiral waves, the dynamical behaviors of local points are the same. However, in the final structure of the CSWs, the dynamical behavior of the local points in the SS is different from that in the BS. This is attributed to the presence of both SSW and OUT-SSW in the CSWs. Specifically, when d is in the interval $[1.5000, 1.5201]$ [corresponding to the spiral wave in Fig. 3(a)], period-5 states of local points in the SSW and OUT-SSW both move clockwise along invariant circles in the phase space. When d is in the interval $[1.5202, 1.5234]$ [corresponding to the spiral wave in Fig. 3(b)], period-5 states of local points in the SSW move clockwise in the phase space, and period-5 states of local points in the OUT-SSW are static. When d is in the interval $[1.5235, 1.5437]$ (corresponding to common outward-propagating spiral waves), period-5 states of local points in the SSW and OUT-SSW move clockwise and counterclockwise in the phase space, respectively. When d is in the interval $[1.5438, 1.5446]$ [corresponding to the spiral wave in Fig. 3(c)], period-5 states of local points in the SSW are static, and period-5 states

of local points in the OUT-SSW move counterclockwise in the phase space. When d is in the interval $[1.5447, 1.5540]$ (corresponding to the inward-propagating spiral waves and CSWs), period-5 states of local points in the SSW and OUT-SSW both move counterclockwise in the phase space.

In the spatially homogeneous system without diffusion coupling, the period-5 states of local points will stabilize at the period-5 orbits. However, in spiral waves, the period-5 states of local points can move along a closed curve in the phase space. Accordingly, in spiral waves, there are effects that cause period-5 states to move along an invariant circle. We termed the effect the move state effect (MSE), denoted as I . In fact, Fig. 4 shows two types of MSEs which cause the movements of period-5 states. One type originates from the diffusive coupling at the boundaries between neighboring cells, denoted as I_b , causing the movement of the boundaries, and the other type originates from the center of spiral waves, denoted as I_c . The effect of I_c propagates outward from the center of the spiral wave through the SSW. Local points in the OUT-SSW are only affected by I_b , while local points in the SSW are jointly affected by I_b and I_c . The dynamical behaviors of local points in the SSW shown in Fig. 4 are the results of the combined effect of I_b and I_c . When I_b disappears, I_c becomes apparent, such as the formation process of spiral waves in Fig. 3(b). When I_b and I_c are opposite in direction and equal in size, the period-5 states of the local points in SSW will be stationary in the phase space [see Fig. 4(d)]. Therefore, we believe that the rich dynamical behaviors of spiral waves shown in Fig. 2 should be the results of the combined effect of I_b and I_c . Since the dynamical behaviors of local points in the OUT-SSW are exclusively determined by I_b , it can be inferred from Fig. 4 that I_b can be managed by altering the parameter d . It is evident that the direction of I_b can be altered by altering the parameter d , as indicated by the bigger black arrows. Specifying the counterclockwise direction as the positive direction, if I_b is greater than 0, the direction follows the counterclockwise path, and if I_b is less than 0, it follows the clockwise direction. We included a quantitative method for I_b in our analysis results and carried out quantitative calculations. In addition to understanding the relationship of I_b and d , it is also necessary to know the relationship of I_c and d .

Figure 5 depicts I_c in the phase space with $d = 1.55$. The white closed curve is the invariant circle of the local points in the OUT-SSW, and the white point inside it is a fixed point $U_0(0, 0)$ (unstable focus). Our analysis results included a stability analysis of the fixed point. Inside the white closed curve, period-5 states undergo an outward clockwise spiral movement centered on the fixed point U_0 . The states of the local points at the spiral center are at the fixed point U_0 . Due to diffusive coupling, the states of local points near the spiral center are subjected to an effect directed towards U_0 [see the red arrows in the inset of Fig. 5]. As shown in the inset, the black curves represent the directions of local dynamics of the period-5 states without diffusive coupling. The combined effect of these two effects is I_c , which makes the states move clockwise around U_0 in the phase space. In spiral waves, the effect of I_c can propagate outward from the spiral center through diffusive coupling. The results also indicate that there is no significant

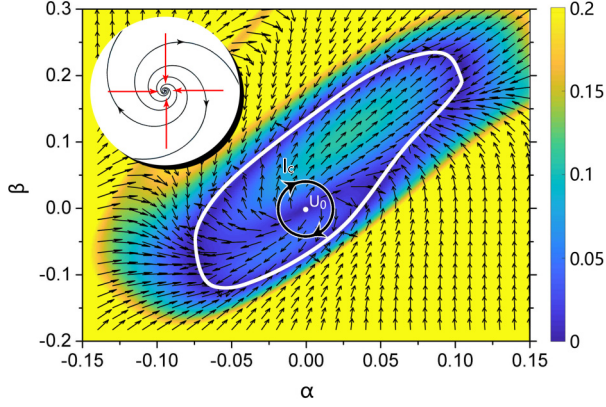


FIG. 5. I_c in the phase space with the parameter $d = 1.55$. The color bar and clusters of black arrows represent the relative size and direction of local dynamics without diffusive coupling, respectively. The bigger black arrows indicate I_c . The white closed curve is the invariant circle of the period-5 states of local points in the OUT-SSW. Inset: schematic diagram for the formation mechanism of I_c .

change in I_c within the parameter interval we considered. The relative size and direction of local dynamics without diffusive coupling remain unchanged when the parameter d changes [see Fig. S2]. Therefore, we assume that I_c remains unchanged within the parameter interval we considered. By examining Fig. 4(d), which shows the relationship between I_b and I_c , we can deduce I_c indirectly, as it is equal to the negative of I_b .

IV. ANALYTICAL RESULTS

Here, we first analyze the stability of the period-5 orbits. Then, based on the characteristics of the period-5 orbits, the mechanism and quantitative method of I_b are proposed. Finally, we explain the formation mechanism of the patterns.

A. Stability analyses of the period-5 orbits

Due to the spatially homogeneous system of Eq. (5) exhibiting period-5 oscillations in the parameter interval ($1.500 \leq d \leq 1.554$), we need to calculate the period-5 orbits and analyze their stabilities. The spatially homogeneous system can be represented as

$$\mathbf{X}_{n+1} = \mathbf{G}_h(\mathbf{X}_n) = \begin{bmatrix} f(\alpha_n, \beta_n) \\ g(\alpha_n, \beta_n) \end{bmatrix}. \quad (11)$$

Period-5 states of the spatially homogeneous system can be described by

$$\mathbf{X}_{n+5} = \mathbf{G}_h^5(\mathbf{X}_n). \quad (12)$$

Then period-5 orbits of the spatially homogeneous system satisfy $\mathbf{X}_{n+5} = \mathbf{X}_n$. Take the case in which the parameter d is equal to 1.55 as an example. A total of 11 period-5 orbits

were obtained, i.e.,

$$\begin{aligned} U_0 &= [\alpha, \beta]^T = [0, 0]^T, \\ U_1 &= [0.1046, 0.2107]^T, & S_1 &= [0.1047, 0.1914]^T, \\ U_2 &= [0.0451, 0.0268]^T, & S_2 &= [0.0345, -0.0038]^T, \\ U_3 &= [-0.0215, -0.0960]^T, & S_3 &= [-0.0376, -0.1120]^T, \\ U_4 &= [-0.0732, -0.0785]^T, & S_4 &= [-0.0745, -0.0486]^T, \\ U_5 &= [-0.0030, 0.1298]^T, & S_5 &= [0.0284, 0.1805]^T, \end{aligned}$$

where $S_2 = \mathbf{G}_h S_1$, $S_3 = \mathbf{G}_h S_2$, $S_4 = \mathbf{G}_h S_3$, $S_5 = \mathbf{G}_h S_4$, $S_1 = \mathbf{G}_h S_5$, $U_2 = \mathbf{G}_h U_1$, $U_3 = \mathbf{G}_h U_2$, $U_4 = \mathbf{G}_h U_3$, $U_5 = \mathbf{G}_h U_4$, $U_1 = \mathbf{G}_h U_5$, and $U_0 = \mathbf{G}_h U_0$. To analyze the stability of the period-5 orbits, we need to study the corresponding characteristic equations, eigenvalues, and eigenvectors.

One can obtain the matrix

$$\begin{aligned} \mathbf{J}_p(\mathbf{X}_n) &= \mathbf{J}(\mathbf{X}_{n+4})\mathbf{J}(\mathbf{X}_{n+3})\mathbf{J}(\mathbf{X}_{n+2})\mathbf{J}(\mathbf{X}_{n+1})\mathbf{J}(\mathbf{X}_n) \\ &= \begin{bmatrix} W_{1,1} & W_{1,2} \\ W_{2,1} & W_{2,2} \end{bmatrix}, \end{aligned} \quad (13)$$

where \mathbf{J} is the Jacobian matrix of Eq. (11). $\mathbf{J}_p(\mathbf{X}_n)$, the product of $\mathbf{J}(\mathbf{X}_n)$, $\mathbf{J}(\mathbf{X}_{n+1})$, $\mathbf{J}(\mathbf{X}_{n+2})$, $\mathbf{J}(\mathbf{X}_{n+3})$, and $\mathbf{J}(\mathbf{X}_{n+4})$, is the Jacobian matrix of Eq. (12) at the period-5 orbit \mathbf{X}_n . The characteristic equation is

$$\lambda^2 - (W_{1,1} + W_{2,2})\lambda + \begin{vmatrix} W_{1,1} & W_{1,2} \\ W_{2,1} & W_{2,2} \end{vmatrix} = 0. \quad (14)$$

The eigenvalues and eigenvectors corresponding to the 11 period-5 orbits can be obtained, as shown in Table I. So we obtained the stabilities of these orbits. U_0 is an unstable focus. U_1, U_2, U_3, U_4, U_5 are saddles, and S_1, S_2, S_3, S_4, S_5 are stable nodes.

The flow trajectory of period-5 states near these nodes and saddles can be described by

$$\frac{\ln |\alpha|}{\ln \lambda_1} - \frac{\ln |\beta|}{\ln \lambda_2} = C, \quad (15)$$

where λ_1 and λ_2 are the eigenvalues corresponding to the nodes and saddles in Table I. C is a constant determined by the points that the curve passes through [see Fig. S3 for the trend of period-5 states near the saddles [51]]. When λ_1 and λ_2 are conjugated to each other, they can be written in the form $\lambda_1 = \lambda_2^* = \sqrt{\lambda_1 \lambda_2} e^{i\vartheta}$ ($0 < \vartheta < \pi$). Then the equation describing the flow trajectory of period-5 states near the unstable focus is

$$\rho \exp\left(\frac{-\theta \ln \sqrt{\lambda_1 \lambda_2}}{\vartheta}\right) = C, \quad (16)$$

where ρ and θ are the polar radius and angle of polar coordinates with the focus as the pole, respectively. C is a constant determined by the points that the curve passes through.

Figure 6 shows the phase portrait of period-5 states when the parameter d is equal to 1.55. The stable nodes are represented by black solid circles, and the unstable focus and saddles are represented by red open circles. Period-5 states gradually tend to one of the stable nodes and stabilize at it eventually. When a diffusive coupling occurs between states at adjacent stable nodes, the states may cross the middle saddle and flow to another stable node. For example, when the states

TABLE I. The eigenvalues of the Jacobian matrix at a fixed point, where λ_1 and λ_2 denote eigenvalues, and i^2 is equal to -1 . \mathbf{u} and \mathbf{v} are the eigenvectors corresponding to λ_1 and λ_2 , respectively.

Fixed point	λ_1, \mathbf{u}	λ_2, \mathbf{v}
U_0	$1.9042 + 0.7318i,$ $\begin{bmatrix} 0.3520 - 0.3092i \\ 0.8835 + 0.0000i \end{bmatrix}$	$1.9042 - 0.7318i,$ $\begin{bmatrix} 0.3520 + 0.3092i \\ 0.8835 + 0.0000i \end{bmatrix}$
U_1	$-0.4860,$ $[-0.4958, -0.8084]^T$	$1.2181,$ $[0.1528, -0.9883]^T$
U_2	$-0.4909,$ $[-0.4269, 0.9043]^T$	$1.2147,$ $[-0.3284, -0.9446]^T$
U_3	$-0.4856,$ $[0.4116, 0.9114]^T$	$1.2205,$ $[0.6842, 0.7293]^T$
U_4	$-0.4869,$ $[-0.9978, -0.0662]^T$	$1.2186,$ $[0.0851, 0.9964]^T$
U_5	$-0.4875,$ $[0.2524, 0.9676]^T$	$1.2187,$ $[0.5174, 0.8558]^T$
S_1	$-0.2013,$ $[-0.4717, -0.8818]^T$	$0.7188,$ $[-0.1510, -0.9885]^T$
S_2	$-0.1993,$ $[0.1133, 0.9936]^T$	$0.6948,$ $[0.3260, 0.9454]^T$
S_3	$-0.2002,$ $[0.5440, 0.8391]^T$	$0.7159,$ $[0.7333, 0.6799]^T$
S_4	$-0.2008,$ $[0.0108, -0.9999]^T$	$0.7162,$ $[-0.5553, 0.8316]^T$
S_5	$-0.2015,$ $[0.3819, 0.9242]^T$	$0.7162,$ $[0.5319, 0.8468]^T$

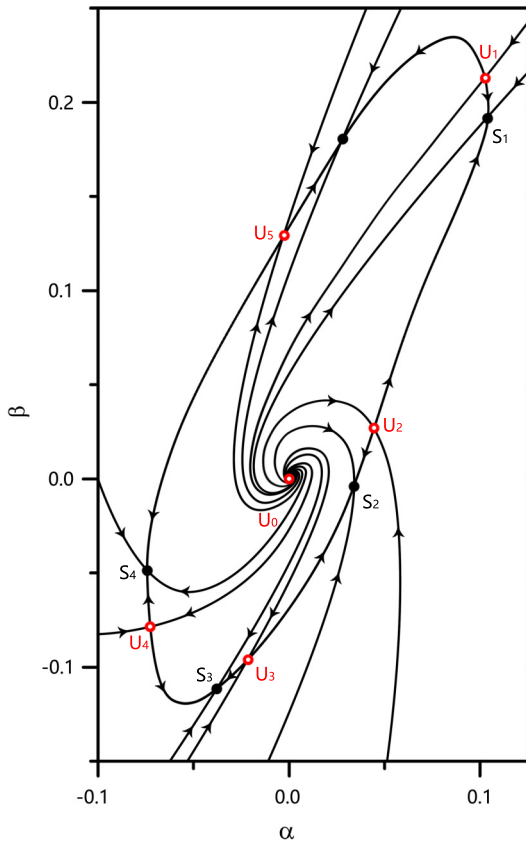


FIG. 6. Phase portrait of period-5 states with the parameter $d = 1.55$. Black solid and red open circles are the period-5 orbits.

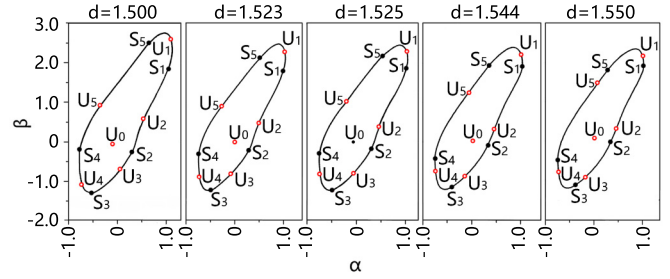


FIG. 7. The invariant circle and fixed points of period-5 states with different values of the parameter d .

in S_3 and S_2 are coupled, the states in S_3 will cross U_3 and flow to S_2 . This type of coupling occurs between the states of local points at the boundaries between neighboring cells in spiral waves. Accordingly, I_b is attributed to this type of spatial distribution of stable nodes and saddles. As a result, period-5 states of local points at the boundaries can move along the invariant circle, as shown in Fig. 4. And the movement of period-5 states of local points at the boundaries is manifested as the movement of the boundaries.

B. Move state effects: I_b and I_c

To explain the change in the direction of I_b shown in Fig. 4, we need to find the period-5 orbits corresponding to different values of the parameter d . Figure 7 shows the positions of the period-5 orbits in the phase space when the parameter d takes different values (corresponding to the five intervals in Fig. 4, respectively). The stability of these orbits was analyzed. The fixed points U_0 are all unstable focuses, and U_1, U_2, U_3, U_4, U_5 are saddles. When the parameter d is less than or equal to 1.530, the fixed points $S_1, S_2, S_3, S_4,$ and S_5 are stable focuses. When the parameter d is greater than 1.530, $S_1, S_2, S_3, S_4,$ and S_5 are stable nodes. Therefore, the stability characteristics of the system as a whole do not change in the interval considered in this paper. From these results, we can understand the change in the direction of I_b . For instance, with the parameter $d = 1.500$, when the states in S_3 and S_2 are coupled, the state in S_2 will pass U_3 and flow to S_3 , thus making states move clockwise along the invariant circle. When the parameter d is equal to 1.523, because the distances from U_3 to S_3 and S_2 are the same, the original state in S_3 or S_2 cannot pass U_3 and flow to another stable node, so states cannot move. When the parameter d is equal to 1.535, 1.544, and 1.550, with the coupling of states in S_3 and S_2 , the original state in S_3 will pass U_3 and flow to S_2 , thus making states move counterclockwise along the invariant circle. Accordingly, we can quantify I_b according to the relative position relationship of period-5 orbits in the phase space, i.e.,

$$I_b := \frac{1}{5} \sum_{j=1}^5 \frac{L(S_j, U_{j+1}) - L(S_{j+1}, U_{j+1})}{L(S_j, S_{j+1})}, \quad (17)$$

where the operation $L(A, B)$ indicates the Euclidean distance between points A and B in the (α, β) plane. S_6 and U_6 denote S_1 and U_1 , respectively. States move counterclockwise when I_b is greater than 0, and clockwise when I_b is less than 0. Note

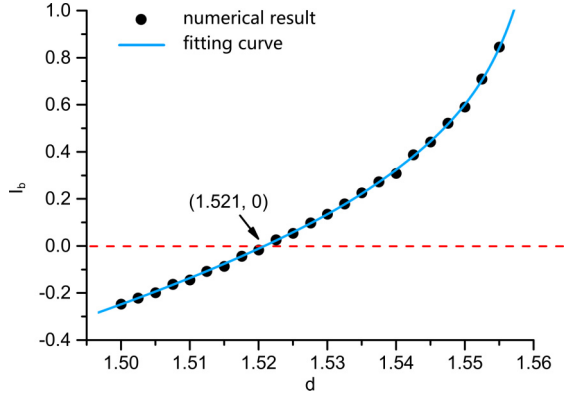


FIG. 8. I_b as a function of the parameter d . The red dotted line represents the horizontal straight line $I_b = 0$. When the parameter d is approximately 1.521, the corresponding value of I_b is equal to 0.

that only when $|I_b|$ is greater than a threshold value can period-5 states move.

According to the definition of I_b , the relationship between I_b and the parameter d can be obtained, as shown in Fig. 8. The results are in good agreement with the dynamic behaviors of local points in the OUT-SSW [see Fig. 4]. That is, when the parameter d is in the interval $[1.5202, 1.5234]$, I_b is too small to move the period-5 states. When d is in the interval $[1.5000, 1.5201]$, I_b is less than 0, making the period-5 states move clockwise in the phase space. Conversely, when d is in the interval $[1.5235, 1.5540]$, I_b is greater than 0, making the period-5 state move counterclockwise. The fitting curve for the relationship between d and I_b is

$$I_b(d) = 0.194 \exp(0.983d) - 0.111 \exp(-0.651d). \quad (18)$$

As shown in Fig. 4(d), period-5 states of the local points in the SSW are at rest in the phase space, because these local points are simultaneously affected by I_b and I_c in opposite directions and of similar sizes. Since I_c is a constant, we can use the relationship between I_b and I_c to get the value of I_c , that is, $I_c \approx -I_b(1.5442) = -0.3522$.

Based on the above analysis, we can clearly explain the dynamical behaviors of local points in the SSW shown in Fig. 4. When d is in the interval $[1.5000, 1.5437]$, $\bar{I} := I_b + I_c$ is less than 0, so period-5 states of the local points in the SSW move clockwise in the phase space. When d is in the interval $[1.5438, 1.5446]$, \bar{I} is approximately equal to 0, so the period-5 states are at rest in the phase space. When d is in the interval $[1.5447, 1.5540]$, \bar{I} is greater than 0, so the period-5 states rotate counterclockwise in the phase space. That is, the dynamical behaviors of local points in the SSW are determined by \bar{I} . Consequently, we explained the effect of the parameter d on the period-5 states of local points.

C. Mechanism of the patterns

Furthermore, we can explain the dynamical behaviors of the spiral waves in Figs. 2 and 3. Movements of the boundaries and waves are the external manifestation of the directional transfer of the period-5 states in the phase space. As shown in Fig. 2, when d is in the first interval, the directions of I_b and I_c are the same, ultimately forming the

common spiral waves. When d is in the second interval, I_b and I_c have opposite directions and similar sizes, i.e., $\bar{I} \approx 0$. Therefore, the SSW affected by \bar{I} remains stationary. When d is in the third interval, the directions of I_b and I_c are opposite, and $|I_b|$ is slightly larger than $|I_c|$, i.e., $\bar{I} > 0$. So the period-5 states in the SSW move counterclockwise in the phase space. In this case, the effect of I_c can still spread outwards. Since the period-5 states move counterclockwise in the phase space, the waves propagate toward the center of the spiral wave. When d is in the fourth interval, the effect range of I_c will gradually decrease as d increases, leading to the appearance of the BS and SS. As shown in Fig. 4(e), the speed of boundaries v_b is determined by I_b , and the period of local points in the SSW is jointly determined by I_b and I_c . Then, Eq. (10) can be rewritten as

$$\Phi_{SS} = \frac{v_b(I_b)T_s(I_b, I_c)}{\pi}. \quad (19)$$

Consequently, the diameter of the area occupied by the SS is determined by I_b and I_c .

V. CONCLUSIONS AND DISCUSSIONS

We have studied a novel type of spiral waves, i.e., the CSW, in a discrete-time predator-pest model, and we revealed the formation mechanism. We have defined and quantified the SME of period-5 states. There are two types of SME in the system, one originating from the boundaries of adjacent stable period-5 orbits (denoted as I_b), and the other originating from the spiral center (denoted as I_c). The theoretical values of I_b are strictly consistent with the numerical results. Our results show that the CSWs are the results of the competition between I_b and I_c . For the dynamical behaviors of local points in the SSW, when \bar{I} is less than 0, the period-5 states of the local points move clockwise in the phase space. When \bar{I} is equal to or very close to 0, the period-5 states of the local points are stationary in period-5 orbits. When \bar{I} is greater than 0, the period-5 states of the local points move counterclockwise in the phase space.

In general, the structure of spiral waves changed from simple to complex due to the transition of local dynamics from simple to complex [52], such as the overtargeted spiral waves [28,29] and wavelength-doubled spiral waves [32,33]. However, in this study, although the structure of CSWs becomes complex, the local dynamical behaviors do not change.

Generally, the dynamical behaviors of local points are the same except for the area near spiral tips. In the spiral waves of this article, the dynamical behaviors of local points in the SSW and OUT-SSW are different.

Our findings may predict the spatial distribution of pests and provide guidance for pest control. Spatial explicit models are more realistic than spatial implicit models for ecosystem prediction [48]. The spatiotemporal patterns we observed are the theoretical prediction of the population density distribution of pests in the system. Because spiral waves can self-organize and self-sustain in autonomous systems [1], the spatial distribution of pests in deciduous forests has a high probability of spiral wave patterns.

ACKNOWLEDGMENTS

This work is supported by the International Joint Research Center of Simulation and Control for Population Ecology of Yangtze River in Anhui under Grant No. 12011530158, the Key Laboratory of Modeling, Simulation and Control of Complex Ecosystem in Dabie Mountains of Anhui Higher

Education Institutes under Grant No. ASSL0115, the National Natural Science Foundation of China under Grants No. 12205006 (J.G.), No. 11975025 (C.S.), and No. 11875042 (C.G.), the Excellent Youth Scientific Research Project of Anhui Province under Grant No. 2022AH030107 (J.G.), and the Natural Science Foundation of Anhui Higher Education Institutions of China under Grant No. KJ2020A0504 (X.L.).

-
- [1] Y. Qian, X. Liao, X. Huang, Y. Mi, L. Zhang, and G. Hu, Diverse self-sustained oscillatory patterns and their mechanisms in excitable small-world networks, *Phys. Rev. E* **82**, 026107 (2010).
- [2] A. T. Winfree, Spiral waves of chemical activity, *Science* **175**, 634 (1972).
- [3] A. T. Winfree and S. H. Strogatz, Singular filaments organize chemical waves in three dimensions: I. Geometrically simple waves, *Physica D* **8**, 35 (1983).
- [4] S. Grill, V. S. Zykov and S. C. Müller, Feedback-controlled dynamics of meandering spiral waves, *Phys. Rev. Lett.* **75**, 3368 (1995).
- [5] S. Grill, V. S. Zykov and S. C. Müller, Spiral wave dynamics under pulsatory modulation of excitability, *J. Phys. Chem.* **100**, 19082 (1996).
- [6] A. Cincotti, F. Maucher, D. Evans, B. M. Chapin, K. Horner, E. Bromley, A. Lobb, J. W. Steed, and P. Sutcliffe, Threaded rings that swim in excitable media, *Phys. Rev. Lett.* **123**, 258102 (2019).
- [7] K. J. Lee, E. C. Cox, and R. E. Goldstein, Competing patterns of signaling activity in dictyostelium discoideum, *Phys. Rev. Lett.* **76**, 1174 (1996).
- [8] C. V. Oss, A. V. Panfilov, P. Hogeweg *et al.*, Spatial pattern formation during aggregation of the slime mould dictyostelium discoideum, *J. Theor. Biol.* **181**, 203 (1996).
- [9] Y. A. Astrov, I. Müller, E. Ammelt, and H. G. Purwins, Zigzag destabilized spirals and targets, *Phys. Rev. Lett.* **80**, 5341 (1998).
- [10] M. Bertram, C. Beta, M. Pollmann, A. S. Mikhailov, H. H. Rotermund, and G. Ertl, Pattern formation on the edge of chaos: Experiments with CO oxidation on a Pt(110) surface under global delayed feedback, *Phys. Rev. E* **67**, 036208 (2003).
- [11] S. Nettesheim, A. Von Oertzen, H. H. Rotermund *et al.*, Reaction diffusion patterns in the catalytic CO-oxidation on Pt(110): Front propagation and spiral waves, *J. Chem. Phys.* **98**, 9977 (1993).
- [12] P. Couillet, Spiral waves in liquid crystal, *Phys. Rev. Lett.* **72**, 1471 (1994).
- [13] S. M. Hwang, T. Y. Kim, and K. J. Lee, Complex-periodic spiral waves in confluent cardiac cell cultures induced by localized inhomogeneities, *Proc. Natl. Acad. Sci. (USA)* **102**, 10363 (2005).
- [14] M. Courtemanche, Complex spiral wave dynamics in a spatially distributed ionic model of cardiac electrical activity, *Chaos* **6**, 579 (1996).
- [15] S. V. Kiyashko, L. N. Korzinov, M. I. Rabinovich, and L. S. Tsimring, Rotating spirals in a Faraday experiment, *Phys. Rev. E* **54**, 5037 (1996).
- [16] E. Meron, Pattern formation in excitable media, *Phys. Rep.* **218**, 1 (1992).
- [17] M. C. Cross and P. C. Hohenberg, Pattern formation outside of equilibrium, *Rev. Mod. Phys.* **65**, 851 (1993).
- [18] J. Gao, C. Gu, H. Yang *et al.*, Prediction of spatial distribution of invasive alien pests in two-dimensional systems based on a discrete time model, *Ecol. Eng.* **143**, 105673 (2020).
- [19] A. Karma, Spiral breakup in model equations of action potential propagation in cardiac tissue, *Phys. Rev. Lett.* **71**, 1103 (1993).
- [20] K. H. Tusscher and A. V. Panfilov, Alternans and spiral breakup in a human ventricular tissue model, *Am. J. Physiol.* **291**, H1088 (2006).
- [21] J. Viventi, D. H. Kim, L. Vigeland *et al.*, Flexible, foldable, actively multiplexed, high-density electrode array for mapping brain activity in vivo, *Nat. Neurosci.* **14**, 1599 (2011).
- [22] A. P. Muñuzuri, M. Gómez-Gesteira, V. Pérez-Muñuzuri *et al.*, Parametric resonance of a vortex in an active medium, *Phys. Rev. E* **50**, 4258 (1994).
- [23] B. Sandstede and A. Scheel, Mechanisms for the generation of coherent longitudinal-optical phonons in GaAs/AlGaAs multiple quantum wells, *Phys. Rev. Lett.* **86**, 171 (2001).
- [24] M. Markus, G. Kloss, and I. Kusch, Transition from spirals to defect turbulence driven by a convective instability, *Nature (London)* **379**, 143 (1996).
- [25] A. F. M. Marée and A. V. Panfilov, Spiral breakup in excitable tissue due to lateral instability, *Phys. Rev. Lett.* **78**, 1819 (1997).
- [26] V. K. Vanag and I. R. Epstein, Segmented spiral waves in a reaction-diffusion system, *Proc. Natl. Acad. Sci. (USA)* **100**, 14635 (2003).
- [27] L. Yang, I. Berenstein, and I. R. Epstein, Segmented waves from a spatiotemporal transverse wave instability, *Phys. Rev. Lett.* **95**, 038303 (2005).
- [28] X. Tang, Q. Gao, S. Gong *et al.*, Spiral waves with superstructures in a mixed-mode oscillatory medium, *J. Chem. Phys.* **137**, 214303 (2012).
- [29] X. Tang, Y. He, I. R. Epstein *et al.*, Diffusion-induced periodic transition between oscillatory modes in amplitude-modulated patterns, *Chaos* **24**, 023109 (2014).
- [30] Y. Gong and D. J. Christini, Antispiral waves in reaction-diffusion systems, *Phys. Rev. Lett.* **90**, 088302 (2003).
- [31] M. Yoneyama, S. Maeda, and A. Fujii, Wavelength-doubled spiral fragments in photosensitive monolayers, *J. Am. Chem. Soc.* **117**, 8188 (1995).
- [32] A. Goryachev, H. Chaté, and R. Kapral, Synchronization defects and broken symmetry in spiral waves, *Phys. Rev. Lett.* **80**, 873 (1998).
- [33] A. Goryachev, H. Chaté, and R. Kapral, Transitions to line-defect turbulence in complex oscillatory media, *Phys. Rev. Lett.* **83**, 1878 (1999).
- [34] J. Gao and C. Gu, Super multi-armed and segmented spiral pattern in a reaction-diffusion model, *IEEE Access* **7**, 140391 (2019).

- [35] S. Ahmad, On the nonautonomous Lotka-Volterra competition equation, *Proc. Am. Math Soc.* **117**, 199 (1993).
- [36] X. Tang and X. Zou, On positive periodic solutions of Lotka-Volterra competition systems with deviating arguments, *Proc. Am. Math Soc.* **134**, 2967 (2006).
- [37] Z. Zhou and X. Zou, Stable periodic solutions in a discrete periodic logistic equation, *Appl. Math. Lett.* **16**, 165 (2003).
- [38] X. Liu, A note on the existence of periodic solution in discrete predator-prey models, *Appl. Math. Model.* **34**, 2477 (2010).
- [39] J. Beddington, C. Free, and J. Lawton, Dynamic complexity in predator-prey models framed in difference equations, *Nature (London)* **255**, 58 (1975).
- [40] X. Liu and D. Xiao, Complex dynamic behaviors of a discrete-time predator-prey system, *Chaos Soliton Fract.* **32**, 80 (2007).
- [41] M. Zhao and L. Zhang, Permanence and chaos in a host-parasitoid model with prolonged diapause for the host, *Commun. Nonlin. Sci. Numer. Simul.* **14**, 4197 (2009).
- [42] A. Khan, I. Ahmad, H. Alayachi *et al.*, Discrete-time predator-prey model with flip bifurcation and chaos control, *Math. Biosci. Eng.* **17**, 5944 (2020).
- [43] Y. Fan and W. Li, Permanence for a delayed discrete ratio-dependent predator-prey system with Holling type functional response, *J. Math. Anal. Appl.* **299**, 357 (2004).
- [44] M. Fan and K. Wang, Periodic solutions of a discrete time nonautonomous ratio-dependent predator-prey system, *Math. Comput. Model.* **35**, 951 (2002).
- [45] D. Hu and Z. Zhang, Four positive periodic solutions of a discrete time delayed predator-prey system with nonmonotonic functional response and harvesting, *Comput. Math. Appl.* **56**, 3015 (2008).
- [46] Y. Xia, J. Cao, and M. Lin, Discrete-time analogues of predator-prey models with monotonic or nonmonotonic functional responses, *Nonlin. Anal.-Real* **8**, 1079 (2007).
- [47] W. Yang and X. Li, Permanence for a delayed discrete ratio-dependent predator-prey model with monotonic functional responses, *Nonlin. Anal.-Real* **10**, 1068 (2009).
- [48] W. S. C. Gurney, A. R. Veitch, and I. C. McGeachin, Circles and spirals: Population persistence in a spatially explicit predator-prey model, *Ecology* **79**, 2516 (1998).
- [49] J. Gao, C. Gu, C. Shen *et al.*, Spiral waves in population density distributions of invasive pests in warm-temperate deciduous forest ecosystems, *Europhys. Lett.* **136**, 30005 (2021).
- [50] D. Barkley, A model for fast computer simulation of waves in excitable media, *Physica D* **49**, 61 (1991).
- [51] See Supplemental Material at <http://link.aps.org/supplemental/10.1103/PhysRevE.108.044205> for additional information, Videos 1–10, supplemental figures, and the stability condition of the algorithm. Videos 1–5 demonstrate the formation process of spiral waves in Fig. 1. Videos 6–10 correspond to the contents in Fig. 3.
- [52] O. Kwon, T. Y. Kim, and K. J. Lee, Period-2 spiral waves supported by nonmonotonic wave dispersion, *Phys. Rev. E* **82**, 046213 (2010).